ELECTRO-OPTIC EFFECT–BASED DETECTION OF ZERO-VALUE INSULATORS IN 220 KV TRANSMISSION LINES

Xudong Ma[1,], Ling Jiang[1], Shengfu Wang[1], Shengcheng Dong[1], Yitao Zhang[1], Guangxiuyuan Zhu[1]*
[1]State Grid Qinghai Electric Power Company Electric Power Science Research Institute, Xining 810000, China

Abstract - Zero-value insulators are still difficult to detect in high-voltage transmission lines, because common diagnostic methods often face problems of low efficiency, limited accuracy, and uncertain field applicability. This study proposes an electroluminescence-based visual detection method for zero-value insulators in 220 kV transmission lines. The method combines ZnS:Cu electroluminescent coating optimization, surface electric-field simulation, and live-line experimental validation. A numerical model of the insulator string was established to analyze the surface electric-field distribution under normal and zero-value conditions. The simulation results show that internal insulation degradation causes a clear decrease in the surface electric field of the faulty unit. This field variation can be directly reflected by the luminescent response of the coating. The experimental results further confirm this mechanism. Under normal conditions, the coatings at the characteristic regions of the insulator string emit stable green light. When a zero-value insulator appears, the coating on the faulty unit does not emit light because its local electric field falls below the excitation threshold. This bright–dark contrast agrees well with the simulation results. The main contribution of this work is that it links coating response, surface electric-field distortion, and zero-value diagnosis into one visual criterion. The proposed method provides a clear and non-contact approach for identifying zero-value insulators. It also offers a practical reference for online inspection and condition monitoring of transmission-line insulation.

Keywords: Electroluminescence; Zero-value insulator; Luminescent characteristics; Transmission line.

1. Introduction

In recent years, with the continued advancement of ultra-high-voltage (UHV) transmission technology, China's grid voltage levels have progressed from 500 kV extra-high voltage toward 1000 kV UHV [1], imposing substantially higher requirements on external insulation performance and operation-and-maintenance reliability. As the key components providing both insulation and load-bearing capability for transmission lines, the condition of insulators is directly related to operational safety. By material, insulators can be classified into porcelain, glass, and composite types [2], among which porcelain insulators are the most widely used owing to their high strength and long service life.

Porcelain insulators consist of a ceramic body, cementing adhesive, and metal fittings; however, affected by sintering and bonding processes, micro-voids or fine cracks are prone to form at interfaces. During long-term service, combined environmental erosion and electrical stresses such as power-frequency and transient overvoltages cause gradual degradation of insulation performance [3–4], and may further trigger surface leakage and partial discharge activity. Under the cumulative action of multiple factors, the insulation resistance may continue to decline to a zero-value state and ultimately break down, resulting in short-circuit or grounding faults [5–7], which underscores the urgent need for live-line inspection and condition assessment methods under online operating conditions.

The spark-fork method evaluates insulation performance by applying voltage at close range and observing the breakdown voltage [8], but it is inherently a contact/near-contact operation and poses significant safety hazards at 220 kV and above. The test device may also disturb the local electric field or introduce additional discharge paths, leading to biased diagnostic criteria [9]. Moreover, this method has limited sensitivity to concealed internal defects, resulting in a high risk of missed detections and false alarms and making it difficult to meet the requirements for "online, non-intrusive" inspection.

dx.doi.org/10.17683/ijomam/issue24.16

Infrared (IR) and ultraviolet (UV) imaging provide non-contact complementary approaches: IR identifies hot spots based on temperature-rise differences [10, 11], whereas UV captures signals associated with partial discharge and corona [12, 13]. However, IR performance is affected by ambient temperature, solar radiation, emissivity, and wind speed, leading to reduced reliability under strong sunlight or high-humidity conditions [14–16]. UV imaging is also limited in detecting low-value/zero-value states that have not yet developed pronounced discharge activity. In addition, field inspections are influenced by viewing angle, standoff distance, and occlusion, and thresholds often rely on experience and can fluctuate with operating conditions, thereby constraining the accuracy and repeatability of large-scale screening [17].

Electric-field sensors can measure the spatial electric field around an insulator string and infer abnormalities accordingly [18], but metallic or conductive components in the sensor body and its supporting structure can readily introduce field distortion. When deployed on unmanned aerial vehicles, fluctuations in attitude, wind speed, and relative position introduce systematic errors, limiting accuracy and repeatability, and practical engineering implementation still requires addressing device-induced interference and environment-coupling effects [19, 20].

Compared with the above methods, an electroluminescence-based method has a more direct response to the surface electric field of insulators. The spark-fork method requires close-range operation and may affect the local electric field. IR and UV methods depend on temperature rise or discharge signals, so they may be less sensitive to early zero-value defects. UAV-based electric-field sensing is non-contact, but its result can be affected by flight position, sensor attitude, and surrounding fittings. In contrast, the electroluminescent coating is directly applied to the characteristic surface region of the insulator. It can convert the local surface electric-field change into a visible light response. This feature makes it useful for visual identification of zero-value insulators.

Electroluminescence is a light-emission phenomenon driven by electric-field-induced radiative recombination of charge carriers, featuring fast response, stable signals, and long-range observability [21-23], and it is promising for translating electric-field distributions into visible light for intuitive characterization, which matches the demand for visual condition monitoring of transmission lines. Inorganic systems such as ZnS exhibit high chemical stability, low sensitivity to oxygen and humidity, and ease of fabrication [24], making them suitable for long-term outdoor exposure. Cu+ doping in the ZnS lattice introduces acceptor levels, promoting recombination luminescence and improving luminance stability [25, 26]. Mechanistically, inorganic AC electroluminescence can be categorized into intrinsic and injection types [27], and it may also be influenced by coupled effects of charge polarization and gas-induced luminescence [28]. In general, reducing trap states and enabling more complete carrier release are beneficial for enhancing luminance [29], and carrier transport, temperature effects, and emission waveforms are correlated [30, 31].

Existing studies have achieved electric-field visualization and distortion identification in equipment such as GIS and GIL [32, 33], and have further applied these approaches to the localization of zero-value insulators [34, 35], yet the relatively high critical threshold field of the materials leads to insufficient emission in low-field regions and compromises field applicability. Lowering the threshold electric field and enhancing low-field responsiveness are therefore essential, which can be realized by introducing high-permittivity fillers and by optimizing coating thickness and interfacial structures to regulate local electric-field distribution. Accordingly, this work prepares a ZnS:Cu electroluminescent coating for 220 kV transmission lines and determines its threshold, identifies the optimal coating region by finite-element calculations, validates the response characteristics through live-line experiments, and proposes a visualization-based self-diagnostic scheme for zero-value insulators in 220 kV lines, providing a basis for rapid screening and quantitative assessment in online patrol inspections. The main contribution of this study is the integration of material optimization, surface electric-field simulation, and live-line validation for zero-value insulator detection. The ZnS:Cu electroluminescent coating was optimized by adjusting the coating thickness and BST content. The pin–cement–porcelain junction was then selected as the coating region according to the simulated surface electric field and the excitation threshold of the coating. Finally, the bright–dark response of the coating was verified under a 220 kV operating condition. This work provides a practical visual criterion for identifying zero-value insulators.

2. Basic Regulation Methods for Electroluminescent Materials

2.1 Fundamental Principles

2.1.1 Overview and Definition

Electroluminescence refers to the phenomenon whereby, under an applied electric field or current, charge carriers inside a material gain energy and emit photons through radiative recombination, giving rise to macroscopic light emission. Depending on the material system and excitation mode, electroluminescence can be broadly classified into inorganic electroluminescence and organic

electroluminescence. Typical inorganic representatives include ZnS-, GaN-, and $BaTiO_3$-based inorganic semiconductor systems, whereas organic electroluminescence is mainly based on organic small molecules or polymers with conjugated structures. In comparison, inorganic AC electroluminescence offers advantages such as high stability, fast response, long service life, and strong environmental adaptability, making it more valuable for applications including electric-field distribution monitoring of power equipment and defect identification of insulators.

2.1.2 Microscopic Luminescence Mechanism

The microscopic luminescence process of inorganic AC-EL materials represented by ZnS:Cu can be interpreted and analyzed using band theory in conjunction with defect-state models. Under an external electric field, electrons in the ZnS lattice are excited to higher-energy states, and a fraction of electrons and holes are captured by shallow traps to form bound states. When energetic electrons and holes encounter each other, electrons can be captured into acceptor levels introduced by Cu^{2+} ions, thereby forming excited-state recombination centers. Because the excited state is unstable, the electron ultimately returns to the ground state and releases energy via radiative transition, emitting blue–green fluorescence:

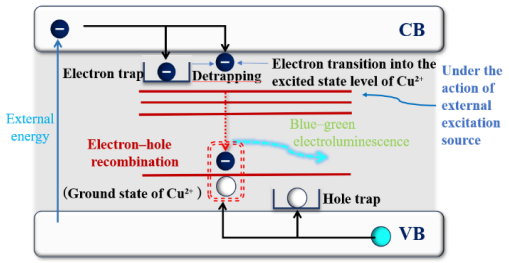

Figure 1: Electroluminescence Mechanism of ZnS:Cu Material

2.1.3 Electroluminescent Image Processing Algorithm

A grayscale-statistics-based luminance analysis algorithm can quantitatively characterize the luminous intensity of an electroluminescent coating after the application of power-frequency voltage, and the algorithm is described as follows. Electroluminescent images of the specimen under different power-frequency voltage amplitudes are captured using an industrial camera, and the color images are converted into grayscale images. The grayscale value is then used to quantitatively represent the luminous intensity, as expressed in Equation (1).

$$G(m,n)=\frac{(B(m,n)+R(m,n)+L(m,n))}{3} \quad (1)$$

To keep the image analysis consistent, all images were processed under the same procedure. The camera parameters were kept unchanged during each group of tests. A non-emitting area in each image was selected as the background region. The background gray value was then subtracted from the original image. The emitting coating area was selected as the region of interest. The maximum gray value and the average gray value in this region were used to describe the luminescence intensity. Each test condition was repeated three times, and the average value was used for comparison.

In Equation (1), $G(m,n)$, $L(m,n)$, $R(m,n)$, and $B(m,n)$denote the grayscale value, green-channel intensity, red-channel intensity, and blue-channel intensity at position (m,n)in the electroluminescent image, respectively. The grayscale value typically ranges from 0 to 255, where 0 represents pure black and 255 represents pure white. A larger grayscale value indicates higher luminous intensity, thereby enabling the grayscale values of the luminescent images to quantitatively characterize the luminance of the electroluminescent coating.

2.2 Methods for Regulating Luminescence Characteristics

2.2.1 Effect of Coating Thickness

During the experiments, five types of electroluminescent coating samples with thicknesses of 0.1 mm, 0.2 mm, 0.3 mm, 0.4 mm, and 0.5 mm were prepared, the thickness range was selected according to coating formability and light-emission stability. A coating thinner than 0.1 mm is difficult to keep uniform on the specimen surface. A coating thicker than 0.5 mm may reduce light extraction and may also affect adhesion. Therefore, the thickness was controlled between 0.1 mm and 0.5 mm in this study. This range can reflect the influence of coating thickness on the luminescent response, following the fabrication procedure shown in Figure 2.

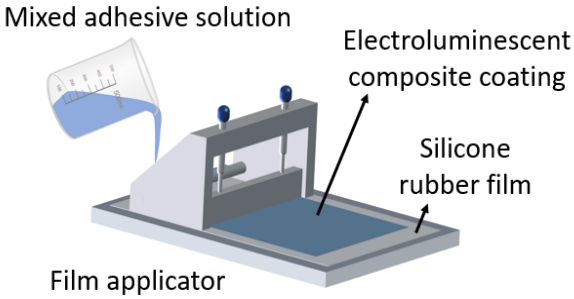

Figure 2: Preparation of ZnS:Cu Coatings with Different Thicknesses

An 8 kV power-frequency voltage was applied to coatings with different thicknesses, and the corresponding electroluminescent images are presented in Figure 3. The comparative results of the maximum luminance grayscale values and the radii of the emitting regions are shown in Figure 4.

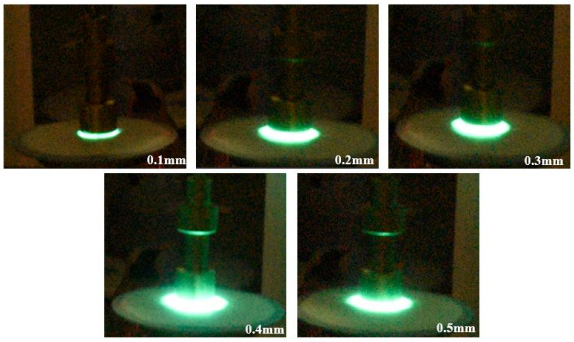

Figure 3: Preparation of ZnS:Cu Coatings with Different Thicknesses

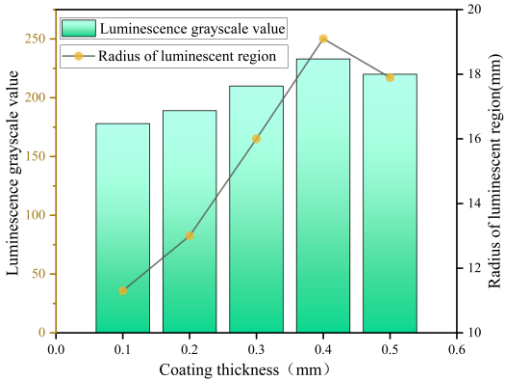

Figure 4: Maximum Luminance Grayscale Value and Emitting-Region Radius of Electroluminescent Coatings with Different Thicknesses

As shown in Figure 3, near the rod electrode, the electric-field intensity is markedly enhanced, so the electroluminescent coating on the specimen surface emits first. Specifically, the region closest to the rod electrode initially emits white light, and with increasing energization time, the emitting area gradually expands outward, forming a dynamic diffusion process from the center to the periphery. Figure 4 further shows the effect of coating thickness on luminescent performance, indicating that the maximum luminance grayscale value "increases first and then decreases" with increasing thickness. At 0.4 mm, the maximum luminance peaks at 230.79. Compared with the 0.1 mm sample, increasing the thickness to 0.4 mm raises the maximum luminance by 31.42% and enlarges the emitting radius by ~7 mm; however, further increasing the thickness to 0.5 mm reduces the luminance by 3.44% and shrinks the emitting radius by 1 mm.

This phenomenon can be attributed to the following mechanism: when the coating is too thin, the number of luminescent centers available for radiative recombination is insufficient, which limits the photon generation rate and consequently reduces the overall luminance. In contrast, when the electroluminescent coating is overly thick, the excessive thickness hinders light extraction from within the coating, thereby diminishing the luminous intensity.

2.2.2 Effect of High-permittivity Particles

The electroluminescent coating uses ZnS:Cu powder as the luminescent core; although emission can be achieved with PRTV as the matrix, its critical threshold electric field is relatively high, leading to low luminance in weak-field regions such as the middle of an insulator string and areas near the crossarm, which is insufficient to support self-diagnosis of zero-value insulators. Therefore, for a given applied power-frequency voltage, it is necessary to enhance the local electric field in the vicinity of the luminescent centers. Because ZnS:Cu has a dielectric constant of approximately 4.5 and is surrounded by a low-permittivity matrix, the electric field tends to be distributed in the matrix rather than the phosphor, which is unfavorable for light emission. High-permittivity BST particles can be incorporated to reconstruct the electric-field distribution and strengthen effective excitation, thereby improving luminance. Accordingly, under an 8 kV power-frequency voltage, the luminance of coatings with ZnS:Cu filler concentrations of 50%–66.7% and BST mass fractions of 0–40% was evaluated, The ZnS:Cu filler concentration was chosen to ensure enough luminescent centers while keeping the coating process workable. The BST content was used to regulate the local electric field around the phosphor particles. A low BST content may have a weak field-enhancement effect. An excessive BST content may reduce the relative amount of ZnS:Cu in the coating. For this reason, the BST mass fraction was set from 0 to 40% to identify a suitable balance between field regulation and luminescent-center density, and the results are shown in Figure 5.

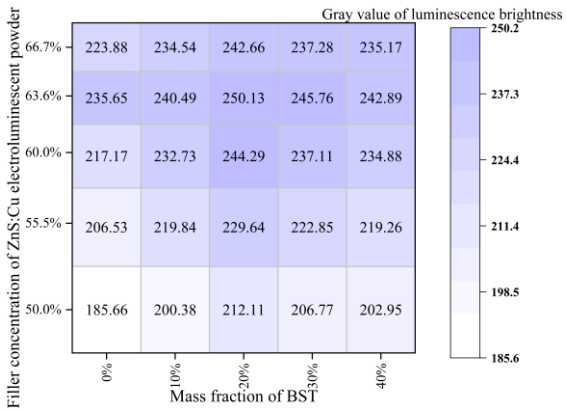

Figure 5: Grayscale Values of Luminescent Images for Different Filler Concentrations and BST Mass Fractions

As shown in Figure 5, the coating exhibits the best luminescence performance at a ZnS:Cu filler concentration of 63.6%. At this concentration, increasing the BST mass fraction from 0 to 20% raises the maximum luminance grayscale value of the electroluminescent coating by 6.14%. With the ZnS:Cu phosphor filler concentration held constant, the maximum luminance grayscale value first increases and then decreases as the BST mass fraction increases.

This behavior primarily arises because introducing BST particles at an appropriate mass fraction increases the overall relative permittivity of the electroluminescent coating, thereby enhancing photon emission intensity under a fixed external electric-field strength. Specifically, the high relative permittivity of BST strengthens the coating's ability to confine electrons and promotes electric-field concentration around the luminescent particles. This facilitates the transition of more electrons from the valence band to the conduction band and their collisions with luminescent centers, exciting the centers to generate more photons and thus increasing the coating's luminance. However, as the BST mass fraction continues to increase, the relative content of ZnS:Cu phosphor in the coating decreases, which reduces the number of luminescent centers per unit volume and leads to a decrease in luminance. Therefore, an optimal BST mass fraction exists, which is 20% in this study, at which the electroluminescent coating achieves the maximum luminance.

3. Finite-Element Simulation Analysis of the Surface Electric Field of a Porcelain Insulator String

In this chapter, a model of a 220 kV transmission-line porcelain insulator string is established, and the spraying location and area of the electroluminescent coating on the insulator surface are determined based on the critical threshold electric field for light emission. Finite-element simulations are performed to analyze variations in the surface electric field of the insulator string under normal operating conditions and under different fault scenarios, including zero-value insulators at various positions.

3.1 Model Development

The porcelain insulator was modeled in SolidWorks, mainly including the porcelain unit, iron cap, pin, and cementing adhesive, and then imported into COMSOL for surface electric-field simulation.

For a 220 kV transmission-line insulator string, the potential at the high-voltage-side conductor was set to 127.02 kV (the phase voltage of a 220 kV line), while the potential at the low-voltage-side crossarm was set to 0 kV.

The three-dimensional structure of the XWP2-70 porcelain insulator is shown in Figure 6.

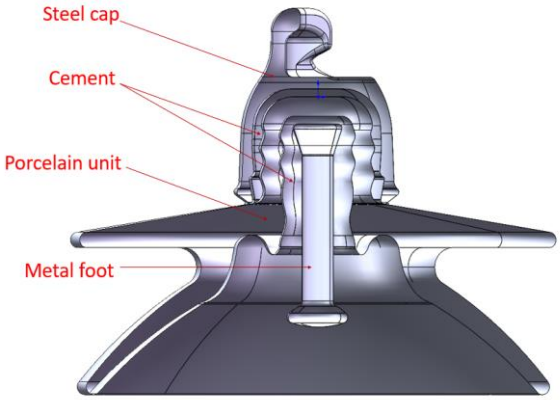

Figure 6: Schematic Diagram of the Porcelain Insulator Structure

The electrostatics module was employed for the simulations, and the solution of the surface electric field of the insulator model should satisfy the electric-field governing equations given in Equations (2)–(3).

$$\nabla \times E = 0 \tag{2}$$

$$\nabla \cdot \varepsilon E = \rho \tag{3}$$

In Equations (2)–(3), Edenotes the electric-field intensity in the dielectric region (kV/m), $\varepsilon$is the relative permittivity of the dielectric, and $\rho$is the space charge density (C/m^3). In the electric-field simulations, the influence of space charge was neglected, and the resulting potential function φsatisfies Equation (4):

$$\nabla^2 \varphi = 0 \tag{4}$$

During the simulation, the experimental model adopts the first-type boundary conditions given in Equations (5)–(6):

$$\varphi|\tau_0 = 0 \tag{5}$$

$$\varphi|\tau_k = U_0 \tag{6}$$

In Equations (5)–(6), $\tau_0$denotes the boundary of the air domain and the ground, whereas $\tau_k$represents the high-potential simulation model; together, Equations (5)–(6) constitute the boundary conditions for the electric-field simulation model.

3.2 Determination of the Spraying Location and Area of the Electroluminescent Coating

In a typical 220 kV transmission-line insulator string, when the surface electric-field intensity exceeds the critical threshold electric field of the electroluminescent material, the electroluminescent coating on the surface will exhibit observable light emission.

According to the voltage-distribution characteristics specified in the DL/T 626-2015 standard, the voltage borne by each unit in an insulator string is non-uniformly distributed, with the minimum voltage reaching several kilovolts and the maximum voltage exceeding the average value per unit. To verify the electric-field distribution of a single insulator unit under power-frequency voltage, a 4 kV power-frequency voltage was applied at the insulator pin, and COMSOL was used to analyze the single-unit insulator. The simulation results are shown in Figure 7.

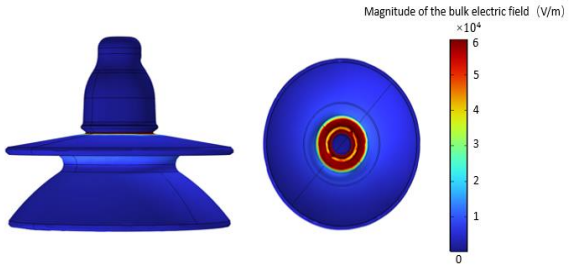

Figure 7: Electric-Field Distribution Contour Map of a Single Insulator Unit under Power-Frequency Voltage

After importing the single porcelain insulator into COMSOL Multiphysics for electric-field distribution simulation, the spatial distribution of the electric-field intensity on the surface and inside the insulator was obtained. The results indicate pronounced differences in electric-field intensity across different surface regions, with notably higher values at the interface between the iron cap and the porcelain body and at the bonding region between the cement and the porcelain near the pin. This is mainly because these two locations are transition interfaces among multiple dielectric materials, where non-uniform permittivity and conductivity increase the local electric-field line density, leading to field distortion and concentration. Since the luminescent response of electroluminescent materials is closely related to the applied electric-field strength, regions with concentrated electric fields can excite luminescent centers more effectively to produce visible radiation.

Accordingly, the interface between the iron cap and the porcelain body, as well as the cement–porcelain interface near the pin, can be selected as typical coating locations for electroluminescent materials to enable visualization of the electric-field distribution and to improve the sensitivity and accuracy of zero-value insulator detection. In summary, the pin–cement–porcelain junction can be regarded as a more suitable characteristic region for spraying electroluminescent materials.

3.3 Surface Electric-Field Distribution of Porcelain Insulator Strings with Zero-Value Units

A zero-value insulator refers to an insulator whose insulation resistance drops below 10 MΩ during service, which may arise from manufacturing-process defects or from long-term environmental effects during operation. During manufacturing, improper control of process parameters—such as sintering temperature, atmosphere, or heating rate—can readily induce microcracks or closed-pore voids at grain boundaries, thereby providing pathways for subsequent electric-field concentration and degradation. In addition, because the constituent materials within an insulator have different thermal expansion coefficients and thermal conductivities, when local regions are subjected to excessive electric-field stress, non-uniform mechanical stress and thermo-mismatch effects between materials can accelerate insulation deterioration, causing the insulation resistance to gradually decrease or even fail. Furthermore, the insulator as a whole can be equivalently modeled as a resistive–capacitive (RC) network, whose equivalent resistance and capacitance vary with material permittivity and conductivity. This directly alters the voltage distribution shared by each unit within the insulator string, causing the surface electric-field intensity to deviate from normal conditions and ultimately promoting the formation of zero-value defects. Contour maps of the surface electric-field distribution of the insulator string under normal 220 kV operation and under a single-unit zero-value condition are shown in Figure 8.

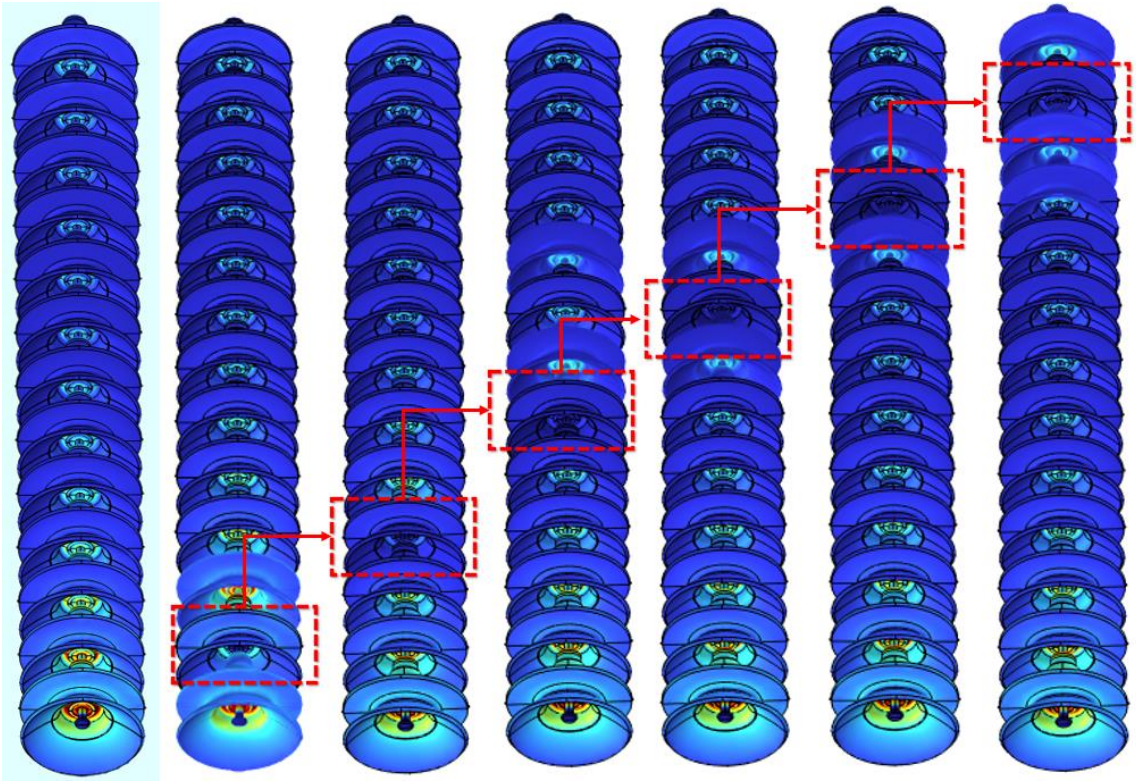

Figure 8: Simulation Map of the Surface Electric-Field Intensity of a 220 kV Insulator String

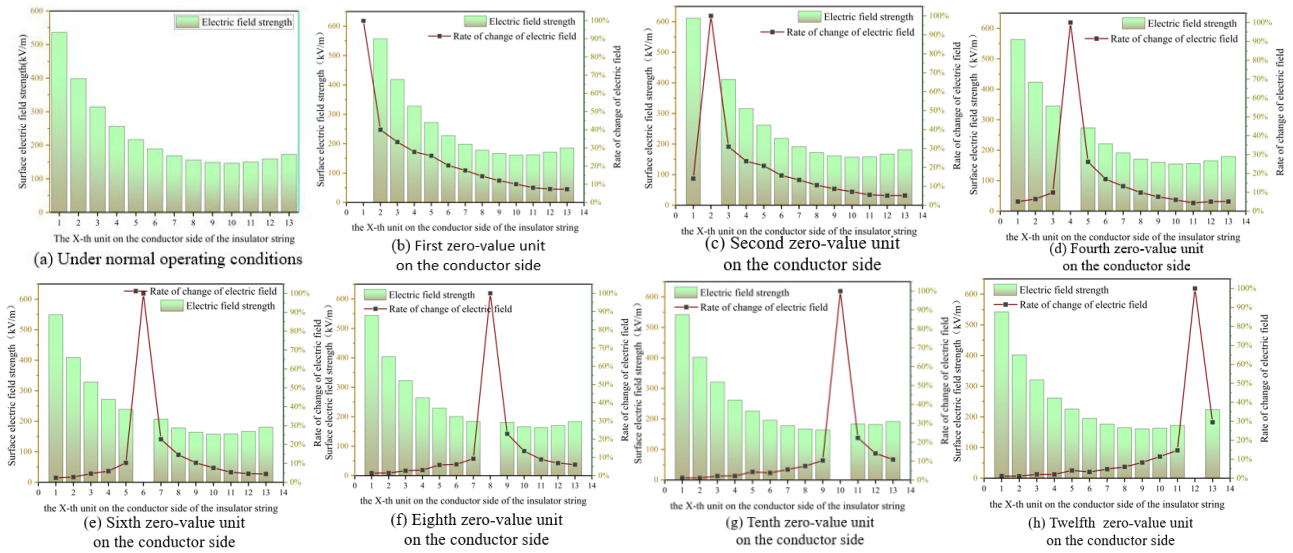

Figure 9: Electric-Field Distribution Contour Map of a Single Insulator Unit under Power-Frequency Voltage

As shown in Figures 8 and 9, from the pin side to the cap side of the insulator string, the surface electric field exhibits an overall saddle-shaped distribution. Because a zero-value insulator has a very low resistance and therefore bears almost no voltage, its surface electric field is nearly zero. When the zero-value insulator is located from the second unit to the twelfth unit, the surface electric-field distribution changes with its position in the string. The results show that a zero-value unit near the high-voltage side has the strongest influence on the surface electric field. The influence becomes weaker when the zero-value unit moves toward the middle and low-voltage sides.

In summary, the electric-field intensity at the cement–porcelain interface in the insulator pin region is sufficient to reach the critical threshold of the electroluminescent coating and can therefore be selected as a preferred characteristic location for coating application. In addition, it is recommended to apply the electroluminescent coating at this interface to ensure the observability and stability of its luminescent response. In subsequent work, the prepared electroluminescent coating will be sequentially sprayed onto the pin–cement–porcelain junction of each unit in the insulator string, and live-line validation tests will be conducted under the actual operating voltage of a 220 kV transmission

line to observe the electroluminescence characteristics of the insulator string and, on this basis, to develop a self-diagnostic method for zero-value insulators in transmission lines based on the electroluminescence effect.

4. Live-Line Experimental Validation of a 220 kV Transmission-Line Insulator String under Different Operating Conditions

Based on the prepared electroluminescent coating and the surface electric-field simulation, this section establishes a 220 kV test platform for zero-value insulators. Live-line tests were carried out under different operating conditions. The experimental results were then compared with the simulation results.

4.1 Experimental Method and Test Platform

The 220 kV transmission-line insulator string consists of 13 porcelain insulator units, each with a resistance of 260 GΩ. A 0.4 mm-thick electroluminescent coating was sprayed at the porcelain–cement interface near the pin of each unit, with a coating width of 10 mm, as shown in Figure 10. The insulation resistances of the zero-value insulators used in the experiment, measured by a megohmmeter, were 6.34 MΩ and 4.93 MΩ, both of which fall within the resistance range for zero-value insulators.

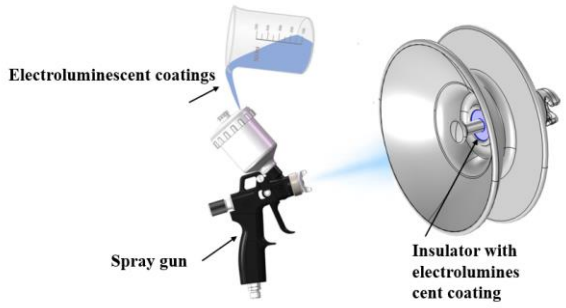

Figure 10: Schematic Diagram of Electroluminescent Material Coating Application

The test platform for zero-value insulators in transmission lines is shown in Figure 10, where one terminal of the power-frequency source is grounded and the other terminal is directly connected to the conductor to apply a power-frequency voltage to the insulator string, with the output voltage regulated by a voltage regulator. The 220 kV transmission-line insulator string was arranged in a suspension configuration, corresponding to the normal condition and the condition with a single zero-value unit within the string, respectively. An industrial camera was used to capture electroluminescent images of the insulator string, with the exposure time fixed at approximately 1 s, the aperture set to 4.5, and the ISO set to 280.

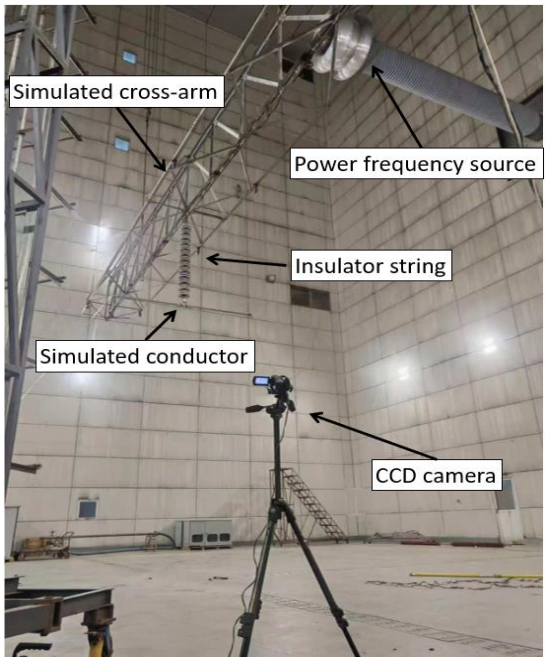

Figure 11: Self-Diagnostic Test Platform for Zero-Value Insulators in Transmission Lines

4.2 Live-Line Test Results of an Insulator String with a Zero-Value Unit under the 220 kV Operating Condition

In this study, a self-diagnostic test platform for transmission-line zero-value insulators based on the electroluminescence effect was established. A typical 220 kV line operating condition was emulated by applying a 127 kV power-frequency voltage, and an electroluminescent coating was applied at the pin regions of the insulator string to observe the electroluminescent responses of a normal string and a string containing a zero-value insulator.

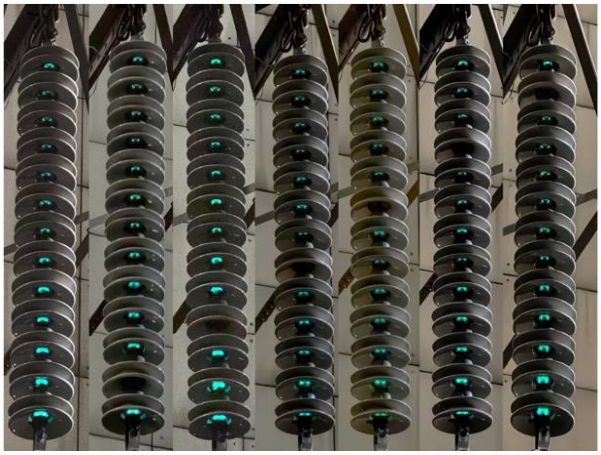

Figure 12: Electroluminescent Experimental Images of the Insulator String under Normal and Single Zero-Value Conditions

As shown in Figure 12, under normal operating conditions, the electroluminescent coating at the pin region of each insulator—i.e., at the porcelain–cement interface—exhibits green emission. This is because, under normal operation, the electric-field intensity at this location exceeds the critical threshold of the electroluminescent coating, allowing the field-supplied energy to drive electronic transitions between excited and ground states while activating luminescent centers to release energy and emit photons. Therefore, in the normal state, the electroluminescent coatings on the surfaces of all units in the string can be excited to produce uniform emission, resulting in an overall bright and homogeneous luminescence distribution.

However, when a zero-value insulator is present in a 220 kV insulator string, the electroluminescent coating on its surface no longer emits light, and the grayscale value at the porcelain–cement interface near the pin decreases markedly, whereas the grayscale values of the coatings on the remaining healthy insulators generally increase. The fundamental reason for this disparity is that the surface electric field of the zero-value insulator is too low to satisfy the energy requirements for electronic transitions and photon emission, leaving its coating in a non-responsive state. Meanwhile, voltage redistribution within the string causes the healthy insulators to withstand higher voltages, thereby increasing their surface electric-field intensities. With the strengthened electric field, the band structure of ZnS:Cu particles in the electroluminescent material shifts toward the Fermi level, and the reduced bandgap facilitates electron transitions and promotes photon emission, leading to a pronounced enhancement in the luminance of the electroluminescent coatings on healthy insulators. This phenomenon reveals the influence of zero-value insulators on voltage distribution and electric-field characteristics, and it provides a physical basis for identifying zero-value insulators using the electroluminescence effect.

4.3 Self-Diagnostic Scheme for Zero-Value Insulators in Transmission Lines

Based on the above analysis, a self-diagnostic method for zero-value insulators in 220 kV transmission lines can be proposed, with the core concept of using the electroluminescence effect to enable visual identification of insulator operating conditions. Specifically, an electroluminescent coating is uniformly sprayed onto the pin region of each unit in the insulator string, i.e., the porcelain–cement interface. Under normal conditions, the electroluminescent coatings on the surfaces of all insulators are excited by the electric field and exhibit a luminescent response, resulting in an overall uniform brightness distribution.

When a zero-value insulator occurs in the string, however, the surface electric field of that insulator cannot satisfy the energy conditions required for light emission, and the electroluminescent coating on its surface becomes non-responsive and no longer emits light, forming a sharp contrast with the brightness of the other healthy insulators. Therefore, once an insulator unit with a non-emitting coating is observed, the presence of a zero-value insulator in the string can be accurately identified.

This scheme shows clear advantages in localization and sensitivity. It can identify zero-value insulators in 220 kV transmission lines through a visible bright–dark contrast. The live-line test results also agree well with the simulated surface electric-field distribution. This agreement suggests that the proposed method has potential for non-contact and online inspection. In practical use, the method may help inspectors locate faulty units more directly and reduce repeated contact tests. However, this study was carried out with a limited number of insulator samples and fault cases. Further field tests are still needed under different voltage levels, pollution conditions, humidity levels, and long-term operating environments. These tests will help verify the stability of the coating and the reliability of the diagnostic criterion.

5. Conclusions

This study proposed an electroluminescence-based visual detection method for zero-value insulators in transmission lines. The luminescent characteristics of ZnS:Cu coatings were first optimized through material regulation. The surface electric-field distribution of a porcelain insulator string was then analyzed by finite-element simulation. Based on the excitation threshold of the coating, the pin–cement–porcelain junction was selected as the coating region. Finally, live-line tests were carried out to verify the visual diagnostic criterion for zero-value insulators.

The luminance of the electroluminescent coating first increases and then decreases with increasing coating thickness, ZnS:Cu phosphor filler concentration, and mass fraction of high-permittivity particles.

The electric-field intensity at the porcelain–cement interface near the insulator pin is higher than the critical threshold electric field of the electroluminescent coating, making it suitable as a characteristic region for coating application.

Under normal conditions, the electroluminescent coating at the porcelain–cement interface near the pin of the insulator string emits light, whereas when a zero-value insulator is present, the coating on the zero-value unit does not emit.

When the zero-value insulator is located on the high-voltage side, it exerts a stronger influence on the electroluminescent coating at the porcelain–cement interface near the pin.

The live-line experimental results are consistent with the surface electric-field simulation results.

Acknowledgement

This work was supported in part by the Science and Technology Project Funding from Qinghai Provincial Electric Power Company (Project No.52280725000H).

References

[1] Li, L., Luo, B., Dong, X., et al. Development status and prospects of high voltage technology. High Voltage Engineering, 2025, 51(08), 3682–3720.
[2] Guan, Z. Insulators and external insulation of power transmission and transformation equipment. Beijing: Tsinghua University Press, 2006.
[3] Gu, X. Research on the formulation, structure, and properties of high-alumina porcelain insulators. Hunan University, 2023.
[4] Wang, X. Research on the degradation mechanism of disc-type suspension porcelain insulators in extremely cold regions. North China Electric Power University (Beijing), 2024.
[5] Liu, P. Study on heating and discharge characteristics of zero-value insulators based on infrared and ultraviolet imaging. North China Electric Power University, 2016.
[6] He, H., Hu, Z., Wang, B., Luo, D., Lee, W.-J., & Li, J. A contactless zero-value insulators detection method based on infrared images matching. IEEE Access, 2020, 8, 133882–133889.
[7] Wu, S. Research on online measurement device for low zero-value porcelain insulators. North China Electric Power University (Beijing), 2010.
[8] Bai, K. Some issues in detecting insulators using spark gaps. High Voltage Engineering, 1993, (03), 53–55.
[9] Zhang, P., Feng, B., & Lu, X. Research on low (zero) value live-line detection method of suspension porcelain insulators. Hong Shui He, 2015, 34(05), 49–52.
[10] Zou, J. Research on zero-value insulator detection based on temperature distribution characteristics. North China Electric Power University (Beijing), 2023.
[11] Wan, Y., Li, N., Li, T., et al. Detection of zero-value insulators in infrared blind spots using disc surface feature recognition. Proceedings of the Chinese Society for Electrical Engineering, 2019, 31(03), 89–95.
[12] Boggs, S. A., Densley, R. J., & Oommen, A. A. UV corona detection for evaluation of outdoor insulators and line hardware. IEEE Transactions on Dielectrics and Electrical Insulation, 2005, 12(6), 1173–1180.
[13] Gholami, F. H., Looms, J. S. T., & Rowland, S. M. Application of ultraviolet imaging for detecting surface discharge on high-voltage insulators. Electric Power Systems Research, 2017, 142, 107–114.
[14] Sun, R., Hu, Y., Jiang, X., et al. Analysis of heating laws and infrared characteristics of degraded porcelain insulators under different pollution conditions. Transactions of China Electrotechnical Society, 2025, 40(11), 3591–3603.
[15] Yin, L., Hu, J., Wang, W., et al. Effect of environmental conditions on zero-value insulator detection criteria using UAV-based infrared inspection. Electric Porcelain Arrester, 2023, (05), 171–177.
[16] Wang, S., Jiang, T., Li, W., et al. Experimental study and coupled-field simulation of infrared and ultraviolet imaging characteristics of zero-value insulator strings. High Voltage Apparatus, 2021, 57(12), 1–9.
[17] Hu, W. Research on defect detection systems for transmission line insulators under complex weather conditions. Anhui University of Science and Technology, 2025.
[18] Gao, S., Jia, J., Huang, X., Liu, Y., Zhang, B., Zhang, Y., & Geng, J. Research on electric field detection of degraded insulators based on a sensitive detection method under complex operating conditions. Applied Sciences, 2022, 12(11), 5680–5697.
[19] Jia, J., Wang, M., Dai, Y., et al. Simulation and detection of spatial electric field distribution of deteriorated insulators in three-phase overhead transmission lines. Journal of Computational Methods in Sciences and Engineering, 2023, 23(3), 1451–1466.
[20] Zhang, D., Wan, W., Liu, X., et al. UAV-based zero-value detection technology for insulators. Electric Power Engineering Technology, 2023, 42(01), 234–242.
[21] Liu, J., Zhang, Z., Liu, Y., et al. Fine-tuned spiral-locked multi-resonant thermally activated delayed fluorescence molecules achieving high-efficiency green electroluminescence close to BT.2020 standard. Science China Materials, 2025, 1–9.
[22] Ma, R., Jia, W., Li, H., et al. Effect of screen printing process on EL device ink layer and luminescent performance. Printing and Digital Media Technology Research, 2025, (04), 81–88.
[23] Zhao, L., Wang, X., Wang, Y., et al. Review of solar cell defect detection using deep learning and electroluminescence imaging. Computer Engineering and Applications, 2025, 1–30.
[24] Harris, P., Den Engelsen, D., Fern, G., et al. AC electroluminescent lamps: Shedding some light on their mysteries. Journal of Materials Science: Materials in Electronics, 2017, 28(10), 7006–7012.

[25] Qi, Y. Theoretical study on electronic structure and optical properties of ZnS doped systems. Qufu Normal University, 2009.

[26] Wang, W. Crystal growth and luminescent properties of powder electroluminescent materials. Hebei University, 2007.

[27] Zhang, Y., Geng, J., Peng, B., et al. Detection method for internal conductive defects in composite insulators based on electroluminescent effect. Proceedings of the CSEE, 2025, 1–13.

[28] Zhu, M., Guo, X., Li, M., et al. Electroluminescent mechanism of ZnS:Cu composite coatings under high electric field. Proceedings of the CSEE, 2023, 43(14), 5693–5703.

[29] Yang, K., Zhang, G., Zhao, W., et al. Study on surface traps and electroluminescence phenomena of polymer insulation materials. Proceedings of the CSEE, 2008, (07), 148–153.

[30] Jia, Y., Ji, S., Yang, X., et al. Voltage sensing characteristics based on electroluminescent effect. Proceedings of the CSEE, 2020, 40(17), 5547–5557.

[31] Ji, S., Jia, Y., Yang, X., et al. Method for measuring electric field distribution along insulator surfaces based on electroluminescence effect and its image processing algorithm. IEEE Transactions on Dielectrics and Electrical Insulation, 2022, 29(3), 939–947.

[32] Yang, X., Jia, Y., Gao, L., et al. Method for measuring insulator surface field strength based on electroluminescent effect. High Voltage Engineering, 2021, 47(04), 1411–1419.

[33] Ji, S., Jia, Y., Yang, X., et al. Method for measuring electric field distribution along insulator surfaces based on electroluminescence effect and its image processing algorithm. IEEE Transactions on Dielectrics and Electrical Insulation, 2022, 29(3), 939–947.

[34] Detection of zero-value insulators using field-induced luminescent screens. Journal of Xi'an Jiaotong University, 1975, (03), 23–30.

[35] Detection of zero-value insulators using field-induced luminescent screens. High Voltage Engineering, 1976, (02), 34–41.